Resonantly enhanced three-photon ionization of krypton

D. B. Geohegan, A. W. McCown,* and J. G. Eden
University of Illinois, Urbana, Illinois 61801
(Received 19 August 1985)

The cross section for three-photon ionization of ground-state krypton at $\lambda = 193$ nm (ArF laser) has been determined. In these experiments, a microwave-absorption technique provided real-time detection of electrons along with measurements of the absolute electron density. Due to a two-photon resonance with the $6p[\frac{3}{2}]_2$ level, the photoelectron number density was observed to vary quadratically with ArF laser intensity for I_{ArF} beyond 50–100 MW cm^{-2} and Kr pressures below 50 Torr.

I. INTRODUCTION

Since the number of visible photons required to photoionize the rare-gas atoms is at least four and the instantaneous laser power is necessarily large, little previous work on multiphoton ionization of these species has been carried out in the visible *or* ultraviolet regions, in particular the measurement of *absolute* photoionization cross sections.

The rare-gas–halide excimer lasers have simplified such studies and the cross section for the two-photon (nonresonant) ionization of Xe at 193 nm has recently been determined.[1] Owing to the large ionization potential of Kr (112 915 cm^{-1} for the $^2P_{3/2}$ state), three photons are required for the photoionization of the atom by an ArF (193 nm) or KrF (248 nm) excimer laser.

For nonresonant photoionization of an atom, the photoelectron production rate varies as I^N where N is the minimum number of photons required to ionize the atom. This process is generally characterized[2] by a small cross section σ. Near 200 nm in krypton, for example, McGuire[3] has calculated σ to be no larger than 10^{-45} cm^6 W^{-2} except in the vicinity of two-photon atomic resonances. Assuming a maximum laser intensity of 250 MW cm^{-2} and a Kr pressure of 50 Torr, the peak electron density that can be produced by nonresonant ionization in this spectral region is $\sim 3\times 10^8$ cm^{-3}. This value is more than two orders of magnitude smaller than the detection limit of the microwave-absorption apparatus used in the present experiments (to be described in Sec. II). Much more efficient production of photoelectrons (10^{11}–10^{12} cm^{-3}) at readily attainable laser intensities (10^8–10^9 W cm^{-2}) requires a resonant or near-resonant interaction in the photoionization process.

This paper describes the results of experiments in which Kr was photoionized at 193 nm by a resonantly enhanced three-photon process. As illustrated in Fig. 1, the large linewidth of an untuned (free-running) ArF oscillator ($\Delta\lambda \sim 0.5$ nm or ~ 140 cm^{-1} full width at half maximum) encompasses three two-photon resonances: $4p^6\,{}^1S_0 \rightarrow 6p[\frac{1}{2}]_0$, $6p[\frac{3}{2}]_2$, and $6p[\frac{5}{2}]_2$. As noted earlier, σ rises sharply at these resonances. However, owing to the nonlinear dependence of the electron production rate for a multiphoton process on laser intensity, the $6p[\frac{5}{2}]_2$ and $6p[\frac{1}{2}]_0$ resonances will be excluded from further consideration because of their position in the wings of the laser's spectral profile. Only the $6p[\frac{3}{2}]_2$ level is assumed to be significantly involved in the photoionization process as the photon fluence at the wavelength for 2γ excitation (193.44 nm) is 0.7 times the peak value (at 193.3 nm).

The analytical problems posed by the presence of the sharp two-photon resonance within a broad laser spectral profile (such as that of the ArF laser involved in these experiments) have stimulated theoretical and experimental interest over the last few years.[4–6] Considering the attractiveness of the rare-gas–halide lasers, in particular, for multiphoton excitation and ionization experiments, it is certainly true that "··· measurements of α [multiphoton excitation cross sections] as a function of bandwidth ··· [are] a fruitful area of research."[7] The difficulty with such measurements is that, since the width of the two-photon resonance cannot readily be measured, the corresponding cross section is difficult to determine. However, in experiments reported here, an *effective* value for the two-photon resonant, three-photon ionization cross section is obtained by measuring the absolute value of the peak electron density as the instantaneous intensity of the ArF laser is varied. The power dependence describing the variation of the photoelectron density with ArF laser in-

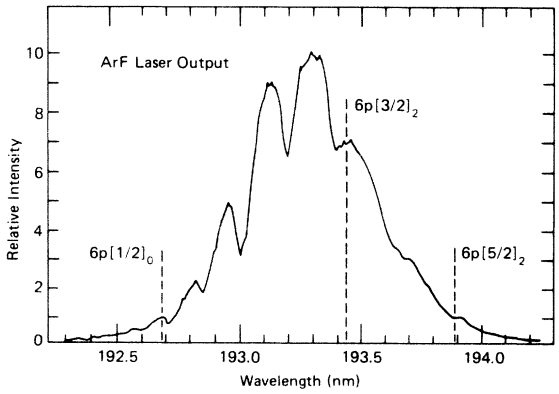

FIG. 1. Spectral overlap between the untuned output of an ArF excimer laser (propagated through air) and the two-photon $4p^6\,{}^1S_0 \rightarrow 4p^5 6p[\frac{5}{2}]_2$, $[\frac{3}{2}]_2$, and $[\frac{1}{2}]_0$ transitions of Kr.

tensity depends on both the Kr pressure and the intensity of the laser. Over most of the laser intensity and pressure ranges explored in these studies, the ionization step in the three-photon process is saturated, which gives rise to a quadratic variation of the photoelectron density n_e with the ArF laser intensity I_{ArF}. However, for $p_{Kr} \gtrsim 50$ Torr and $I_{ArF} \lesssim 100$ MW cm^{-2}, the cubic dependence expected on the basis of perturbation theory is observed. Section II briefly describes the experimental apparatus and the measurements that have been made, while the theoretical framework for the interpretation of the data in terms of an effective cross section is discussed in Sec. III. The results of this work are presented and discussed in Secs. IV and V, respectively, and the conclusions are summarized in Sec. VI.

II. EXPERIMENTAL APPARATUS

The experimental apparatus, shown schematically in Fig. 2, has been described in detail previously.[1] Briefly, the output from an ArF laser (Lambda Physik EMG 150 EST) was focused to a line along the axis of a 22-mm outside-diameter Suprasil quartz cell containing between 10 and 300 Torr of research-grade krypton. The cell was attached to a gas-handling system which allowed for the Kr pressure in the tube to be varied. Great care was taken to ensure cleanliness in the system, including heating the cell with a hydrogen torch and pumping the system to less than 10^{-6} Torr prior to filling with 99.995% Kr. The intensity of the ArF laser pulse was monitored by reflecting 10% of the beam onto a calibrated energy meter and the cross-sectional area of the laser beam at its focus was determined from burn patterns.

A method for determining absolute electron densities from the attenuation of a microwave signal has also been presented previously.[1,8] A klystron operating at 9.08 GHz generated the cw microwave probe signal and isolators prevented the reflection of power back into the klystron. Transitional waveguide sections coupled the rectangular X-band guide (WR90) to a cylindrical segment (slotted to permit entry of the laser beam) which contained the optical cell. A small hole (6 mm in diameter) drilled in an E bend allowed fluorescence measurements on $5p \rightarrow 5s$ and $6p \rightarrow 5s$ transitions (at 760.2 and 446.3 nm, respectively) to be made. Spectroscopic studies were carried out using an optical imaging system in conjunction with a 0.5-m spectrograph and photomultiplier.

Because of the possible presence of Fabry-Perot effects,[9] two types of optical cells were constructed. In order to observe laser-induced fluorescence, a cylindrical cell with plane-parallel windows (sealed on each end of the cell) was used, while a second tube with ends drawn by the glass blower down to a point was employed for the electron density measurements. The latter cell eliminates the Fabry-Perot resonances observed in Ref. 9 and allows for the optimal transmission of the microwave signal through the cell over the full operating range of the klystron.

The transmitted microwave field was detected by a silicon diode and the attenuation waveforms were displayed on a Tektronix 7834 storage oscilloscope. In the absence of electrons in the optical cell, the detector generated a negative 460-mV dc signal. Calibration of the diode consisted of determining the degree of deviation from the dc value for a known attenuation in the microwave signal.

As alluded to earlier, the minimum electron density detectable with this apparatus is $\sim 5 \times 10^{10}$ cm^{-3}. Consequently, nonresonant photoionization processes are not observable. A cross section of 5×10^{-43} cm^{6}W^{-2} would be required for the three-photon (nonresonant) process to contribute 10% of the total electron density that is produced by a 250-MW cm^{-2} ArF (193 nm) laser pulse.

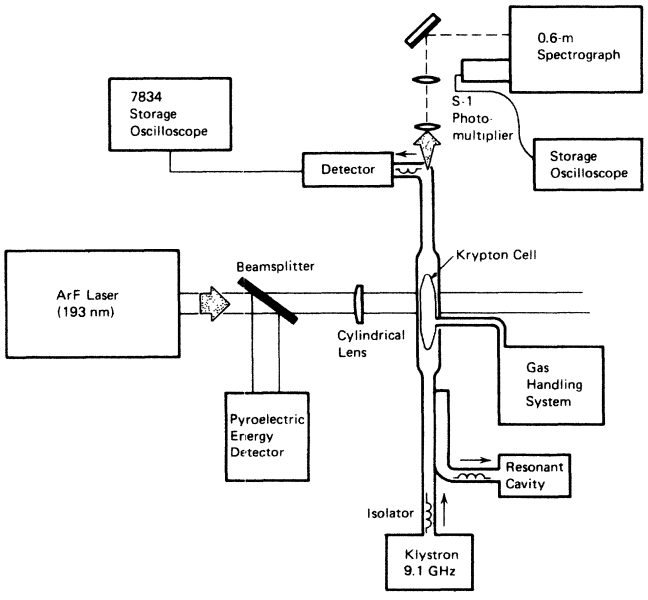

FIG. 2. Schematic diagram of the experimental apparatus. After being filled and sealed, the optical cell was installed in a section of cylindrical waveguide.

III. THEORETICAL CONSIDERATIONS

Previous papers[1,8,9] have discussed the effects of both high-pressure (where the collision frequency ν_m is nearly equal to the microwave frequency ω) and low-pressure ($\nu_m \ll \omega$) background (buffer) gases on the attenuation and phase shift of a microwave field propagating through a weakly ionized plasma. In the high-pressure regime, electrons transfer energy to the gas through elastic collisions, causing an attenuation of the field. Both the phase shift and the attenuation are dependent on the plasma frequency ω_p, which is related to the electron density ($\omega_p^2 = n_e e^2/\epsilon_0 m$). At low pressures, where collisions occur only after a larger number of field oscillations, the electrons oscillate $\pi/2$ out of phase with respect to the field and either shift its phase ($\omega_p < \omega$) or reflect it ($\omega_p > \omega$). The experiments described here involved combinations of krypton pressure and electron energy such that $\nu_m \simeq \omega$.

The electron density that is present at the focus of the ArF beam can be calculated from the measured amount of attenuation α of the microwave field using the expression

$$F\omega_p^2 = 2\alpha^2 c^2 \frac{\nu_m^2+\omega^2}{\nu_m^2}\left[-1+\left[1+\frac{\nu_m^2}{\alpha^2\omega^2}(\alpha^2+\beta_g^2)\right]^{1/2}\right], \tag{1}$$

where β_g is the propagation constant in the cylindrical waveguide (including the quartz cell), c is the speed of light, and F is a scaling factor which reflects the fact that the electrons are produced in a sheet focused at the axis of the cell and attenuation only takes place where electrons are present. Specifically,

$$F=\frac{\int_s f(x,y)E_0^2\,dS}{\int_s E_0^2\,dS}, \tag{2}$$

where the integral is taken over the cross section of the cylindrical waveguide, E_0 is the microwave field amplitude, and $f(x,y)$ is the ratio of the electron density at (x,y) to the value at the focus ($x=0$, with the x axis oriented in the direction of propagation of the ArF beam).

For an N-photon ionization process, the electron density is a function of laser intensity I, photon energy $\hbar\omega$, and gas density (in this case, krypton, [Kr]):

$$n_e=[\mathrm{Kr}]\frac{\sigma\int^\tau I^N dt}{\hbar\omega}=\frac{\sigma[\mathrm{Kr}]}{\hbar\omega}\frac{\int^\tau P^N dt}{A^N}, \tag{3}$$

where σ is the generalized N-photon ionization cross section and the intensity has been written as power per unit area, P/A. Since the area of the beam is its length L times its width W, the electron density at the center of the cell ($x=0$, peak value) is

$$n_p=\frac{\sigma[\mathrm{Kr}]}{\hbar\omega}\frac{\int^\tau P^N dt}{L^N W_0^N} \tag{4}$$

[where τ, the temporal width of the laser pulse at the 10% points, is typically 30 ns and $W(x=0)\equiv W_0$], while the density at a position x (independent of y) is

$$n_e(x)=\frac{\sigma[\mathrm{Kr}]}{\hbar\omega}\frac{\int^\tau P^N dt}{L^N[W(x)]^N} \tag{5}$$

or

$$\frac{n_e(x)}{n_p}=\left[\frac{W_0}{W(x)}\right]^N=f(x,y). \tag{6}$$

Therefore, substituting (6) into (2), one obtains

$$F=W_0^N\frac{\int_s \frac{E_0^2}{[W(x)]^N}dS}{\int_s E_0^2\,dS}. \tag{7}$$

In summary, absolute electron densities are determined by microwave-attenuation measurements from Eq. (1). Both α and β_g are measured and ν_m is inferred from data available in the literature. The values chosen for the latter two constants are discussed in Sec. IV. Also, N and F are known from measurements of the ArF intensity dependence of n_e and the width of the focused laser beam as it traverses the cell, respectively. Therefore, σ can be calculated from Eq. (5).

IV. RESULTS

A. Measurement of β_g

The values of several system parameters necessary for absolute electron density calculations were determined in separate experiments. The propagation constant β_g was measured using a slotted line joined to the cylindrical waveguide which contained only a section of Suprasil tubing. Moving an adjustable short inside the tubing caused a stationary diode in the slotted line to detect periodic nulls in the standing wave. The wavelength in the cylindrical waveguide was determined by measuring the distance which the short had to be moved to observe two nulls. This gave $\beta_g=0.935\ \mathrm{cm}^{-1}$.

B. Atomic fluorescence and ν_m

When the Kr-containing optical cell was irradiated by the ArF laser, strong fluorescence was observed emanating from the $6p[\frac{3}{2}]_2$ state ($6p[\frac{3}{2}]_2\rightarrow 5s[\frac{3}{2}]_2$ and $6p[\frac{3}{2}]_2\rightarrow 5s[\frac{3}{2}]_1$ transitions are at 427.4 and 445.4 nm, respectively) and from lower-lying states (primarily $5p[\frac{1}{2}]_0$, $5p[\frac{3}{2}]_2$, and $5p[\frac{5}{2}]_3$) that are populated from above by quenching. However, no emission was detected from the $6p[\frac{1}{2}]_0$, $6p[\frac{5}{2}]_2$, or $6p[\frac{3}{2}]_1$ states, which supports the contention that the Kr $6p[\frac{3}{2}]_2$ level is the only $6p$ state significantly populated by the two-photon excitation process at 193 nm.

Photoionization of the $6p[\frac{3}{2}]_2$ state ($^2P_{3/2}$ core) by 193-nm photons results in the ejection of either a 5.3- or a 4.6-eV electron, depending on the total angular momentum of the product-ion core. Miller and co-workers[10] have shown that resonant multiphoton ionization in rare gases preferentially produces ions with cores having the same total angular momentum as the intermediate state (in this case, $J=\frac{3}{2}$). Therefore, in determining absolute electron densities, an electron energy of 5.3 eV, corresponding to a $^2P_{3/2}$ ion core, was assumed. Substituting 4.6 eV (for a Kr^+ $^2P_{1/2}$ core) changes the value of the absolute electron density by approximately 20%.

For the gas pressures and laser intensities involved in these experiments, associative ionization of Kr metastables contributes significantly (along with multiphoton ionization) to the overall electron production rate. Therefore, the collision frequency for momentum transfer (ν_m) was not directly measured. However, a value of 2.2×10^9 $\mathrm{s}^{-1}(\mathrm{Torr\ Kr})^{-1}$ was inferred in a manner which has been discussed previously.[1] Since collision frequency is related to gas pressure, electron velocity, and the inelastic collision cross section by the expression

$$\nu_m=[\mathrm{Kr}]\langle\sigma_m v\rangle, \tag{8}$$

where [Kr] is the krypton number density, then once a collision frequency has been measured for one electron energy, it is known at any energy for which the cross section for momentum transfer has been measured. The matter is considerably simplified when the electrons have constant energies, as is the case for photoionization (for time scales short compared to the electron thermalization time at a given gas pressure). For the purposes of this experiment,

a comparison was made between the cross section for momentum transfer (σ_m) for 0.7-eV electrons in xenon (ν_m(Xe)/[Xe] measured to be 3.4×10^{-9} s^{-1}cm^3 (Ref. 1)) and for 5.26-eV electrons in krypton, with the result that σ_m(Kr)/σ_m(Xe)=9.41 (Ref. 11). Therefore,

$$\frac{\nu_m(\mathrm{Kr})}{[\mathrm{Kr}]}=\left[\frac{m_{\mathrm{Kr}}}{m_{\mathrm{Xe}}}\left[\frac{5.26\ \mathrm{eV}}{0.7\ \mathrm{eV}}\right]\right]^{1/2}\frac{\sigma_m(\mathrm{Kr})}{\sigma_m(\mathrm{Xe})}\frac{\nu_m(\mathrm{Xe})}{[\mathrm{Xe}]}$$

$$=7.0\times10^{-8}\ \mathrm{cm^3s^{-1}}\ . \qquad (9)$$

C. Collisional ionization of Kr 5s metastables

For krypton pressures below ~40—50 Torr, the microwave-attenuation (electron density) waveforms behave as expected (cf. Fig. 3). The electron density continues to rise until the ArF laser pulse terminates. Subsequently, n_e falls slowly due to dimerization of Kr^+ ($^2P_{3/2}$) and dissociative recombination of Kr_2^+ $1(\frac{1}{2})_u$. However, for $P_{\mathrm{Kr}}\gtrsim50$ Torr, although an inflection in the waveform occurs at the end of the laser pulse, the maximum electron density is displaced to much later times (~100—150 ns after the arrival of the ArF pulse, depending on P_{Kr}).

Clearly, a fraction of those $6p[\frac{3}{2}]_2$ atomic species produced by the ArF laser relax via collisions [$k_Q(6p[\frac{3}{2}]_2)=6.7\times10^{-10}$ cm^{3}s^{-1} (Ref. 6): $\tau=10$ ns for $P_{\mathrm{Kr}}\sim5$ Torr], which leads to rapid population of the 5s metastable state. As the Kr pressure is increased, the metastable concentration rises until the production of electrons by associative ionization,

$$\mathrm{Kr}(5s)+\mathrm{Kr}(5s)\rightarrow\mathrm{Kr_2^+}1(\tfrac{1}{2})_u+e^-\ , \qquad (10)$$

becomes significant. [The delay in reaching the peak electron density at high Kr pressures ($\gtrsim50$ Torr) that was mentioned above is consistent with reaction (10) if the cross section for the process is assumed to be gas kinetic and if the peak 5s population is at least 1—2% of that in the ground state.] Consequently, the experiments to be described in the following sections were confined to Kr pressures below 50 Torr.

D. Spatial profile of focused ArF laser-beam, effective two-photon cross section

The width of the focusing laser beam was measured from burn patterns taken every 0.1 cm and the following expression, which relates the beam width $W(x)$ at a distance x from the center of the cell to its value at the focus ($x=0$, axis of cell), was derived:

$$W(x)=\begin{cases}0.017+0.575x^2, & 0\le x<0.20\ \mathrm{cm}\\ 0.0066+0.167x, & 0.20\le x\le1.0\ \mathrm{cm}\ .\end{cases} \qquad (11)$$

Note that $W(x)$ is expressed in cm and the length of the ArF beam (i.e., its dimension along the cell's axis) is 3.0 cm. This relation was inserted into Eq. (7) along with an expansion of the electric field in Bessel functions for a TE_{11} mode. After integrating over the cross section of the waveguide, F^{-1} was determined to be 258.

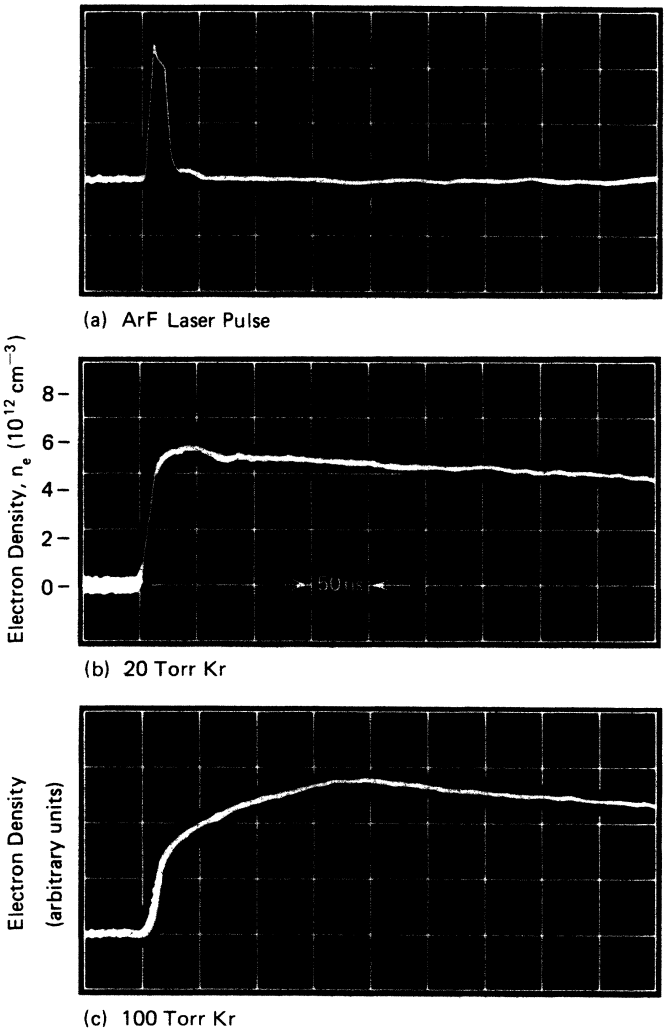

FIG. 3. Laser (a) and microwave-attenuation (b), (c) waveforms observed in these experiments. In (b) and (c) electron density increases vertically, and for Kr pressures beyond ~50 Torr, the influence of metastable-metastable collisions on electron production is clearly evident.

Plots of absolute electron density versus peak ArF laser intensity are given in Figs. 3 and 4 for krypton pressures of 10, 20, and 50 Torr. The solid lines drawn through the data vary quadratically with I_{ArF}, indicating that the multiphoton-ionization process is generally dominated by a two-photon resonance and that the ionization step is saturated. For a particular value of the laser intensity, the electron density is observed to increase linearly with krypton pressure, as expected. Therefore, a value of $N=2$ was used in Eqs. (3)—(7) in determining n_e.

The effective two-photon cross section was calculated from Eq. (4) which describes the electron density at the focus of the beam immediately after the ArF pulse irradiates the gas. Approximating the laser pulse shape by a triangle, the (ArF) intensity is given by

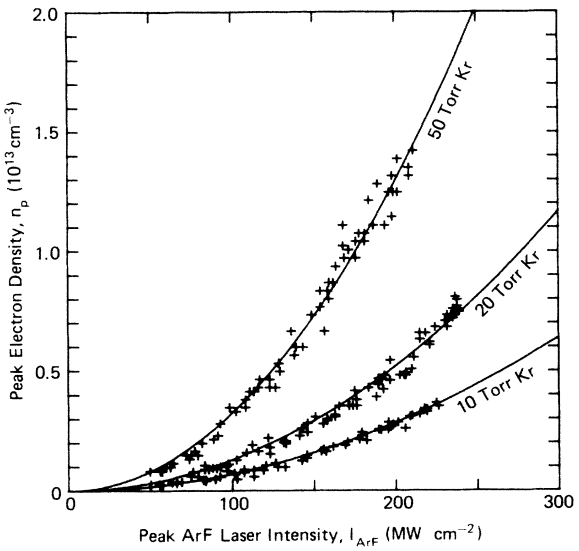

FIG. 4. Laser intensity dependence of the peak photoelectron density for three Kr pressures. The solid lines are computer-calculated, quadratic least-squares fits to the data.

$$I=\begin{cases} I_{\max}\dfrac{t}{t_r} & (0\le t\le t_r) \\ I_{\max}\left[\dfrac{\tau-t}{\tau-t_r}\right] & (t_r\le t\le\tau)\ , \end{cases} \tag{12}$$

where t_r is the rise time of the pulse, $\tau\simeq 30$ ns, and $I_{\max}$ is the peak intensity. Then

$$\int^{\tau} I^2 dt = I_{\max}^2 \tfrac{1}{3}\tau \tag{13}$$

and

$$n_p=\frac{\sigma[\mathrm{Kr}]}{\hbar\omega}\frac{I_{\max}^2\tau}{3} \tag{14}$$

or

$$\sigma=\frac{3\hbar\omega n_p}{[\mathrm{Kr}]I_{\max}^2\tau}\ . \tag{15}$$

From Fig. 3 and Eq. (15), the *effective* two-photon ionization cross section was determined to be 2×10^{-32} cm^4 W^{-1}.

V. DISCUSSION

A. Photoionization and quenching of Kr $6p[\frac{3}{2}]_2$

Assuming a 100-cm^{-1}-bandwidth ArF laser (similar to that involved here), Bokor and co-workers[6] and Bischel *et al.*[5] have estimated the two-photon absorption cross section for the $4p^6\,{}^1S_0\rightarrow 4p^5 6p[\frac{3}{2}]_2$ transition in Kr. Their values [in the range $(1-2.3)\times10^{-31}$ cm^4 W^{-1}] are a factor of 4–10 larger than the measured effective cross section reported here. The order-of-magnitude agreement between the two results is not surprising since the I^2 variation of n_e over most of the range of laser intensities investigated in Figs. 4 and 5 indicates that ionization of the Kr $6p[\frac{3}{2}]_2$ state is saturated (for $P_{\mathrm{Kr}}<50$ Torr and $I>50$ MW cm^{-2}) and the rate-limiting process is two-photon excitation of that intermediate state.

An upper-limit estimate for the photoionization cross section for the $6p[\frac{3}{2}]_2$ state at 193 nm is obtained by *assuming* that the ionization process is saturated even at the lowest intensities studied. Therefore,

$$\frac{\sigma_{\mathrm{PI}} I_{\min}\Delta t}{\hbar\omega}\simeq 1\ , \tag{16}$$

where $I_{\min}\approx 60$ MW cm^{-2} (Fig. 5), Δt (the full width of the laser pulse)$\simeq$25 ns, and σ_{PI} is the $6p[\frac{3}{2}]_2$ photoionization cross section expressed in cm^2. Therefore, σ_{PI} is calculated to be $\sim 6\times10^{-19}$ cm^2. This rough estimate is close to the values reported by Chang and Kim[12] and Bokor *et al.*[6] (8.0×10^{-19} and 3.2×10^{-19} cm^2, respectively).

A more thorough explanation for the quadratic dependence of electron density on laser intensity measured in these experiments is afforded by considering a simple rate-equation model which describes the temporal evolution of n_e and the Kr $6p[\frac{3}{2}]_2$ concentration:

$$\frac{d[\mathrm{Kr}^*]}{dt}=\frac{\sigma I^2}{\hbar\omega}[\mathrm{Kr}]-[\mathrm{Kr}^*]\left[\frac{1}{\tau_{sp}}+k[\mathrm{Kr}]+\frac{\sigma_{\mathrm{PI}}I}{\hbar\omega}\right] \tag{17}$$

and

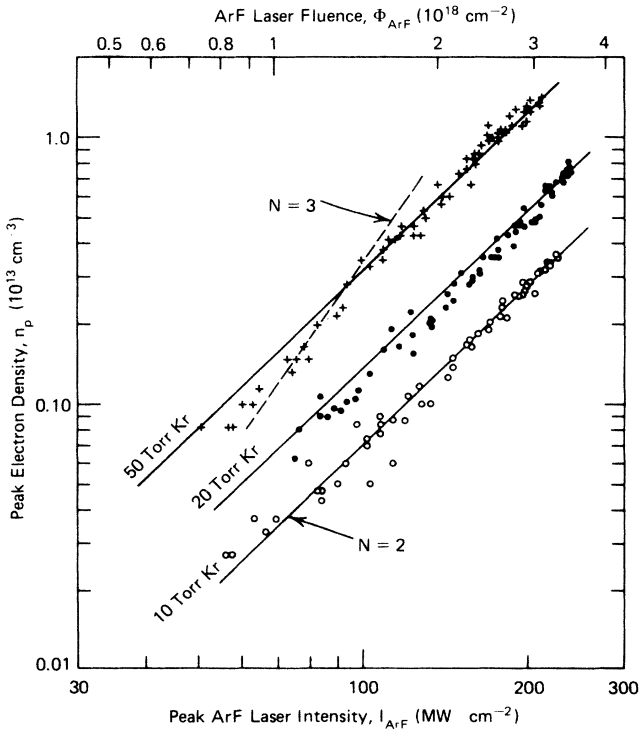

FIG. 5. Same data and least-squares lines as in Fig. 4 but plotted on a semilog scale. The dashed line indicates the near-cubic variation of n_p with laser intensity for the 50-Torr data and $I_{\mathrm{ArF}}\lesssim 100$ MW cm^{-2}.

$$\frac{dn_e}{dt}=\frac{\sigma_{\mathrm{PI}}I}{\hbar\omega}[\mathrm{Kr}^*]\,, \tag{18}$$

where Kr^* denotes the $6p[\frac{3}{2}]_2$ state of Kr, τ_{sp} is the $6p[\frac{3}{2}]_2$ radiative lifetime, and k is the two-body collisional rate constant for quenching of Kr^* by Kr. For the case where the total Kr^* loss rate [the last three terms in (17)] is much greater than $\sigma I^2(\hbar\omega)^{-1}[\mathrm{Kr}]$ (the $6p$ production rate), the peak $6p[\frac{3}{2}]_2$ number density can be expressed as

$$[\mathrm{Kr}^*]=\frac{\frac{\sigma I^2}{\hbar\omega}[\mathrm{Kr}]}{\tau_{sp}^{-1}+k[\mathrm{Kr}]+\frac{\sigma_{\mathrm{PI}}I}{\hbar\omega}}\,. \tag{19}$$

Thus, (18) becomes

$$\frac{dn_e}{dt}=\frac{\sigma_{\mathrm{PI}}I}{\hbar\omega}\frac{\frac{\sigma I^2}{\hbar\omega}[\mathrm{Kr}]}{\tau_{sp}^{-1}+k[\mathrm{Kr}]\frac{\sigma_{\mathrm{PI}}I}{\hbar\omega}}\,. \tag{20}$$

Therefore, in order for the electron density to vary as I^2,

$$\frac{\sigma_{\mathrm{PI}}I}{\hbar\omega}\gg\tau_{sp}^{-1}+k[\mathrm{Kr}]\,, \tag{21}$$

which simultaneously reduces the intensity dependence of the $6p[\frac{3}{2}]_2$ concentration ($[Kr^*]$) to linear. In order to verify this, the fluorescence intensity at 760.2 nm ($5p[\frac{3}{2}]_2\rightarrow 5s[\frac{3}{2}]_2$) was monitored and was indeed found to vary linearly with I_{ArF}. Similarly, for a constant value of I_{ArF}, $[Kr^*]$ should rise linearly with [Kr] until photoionization ceases to be the dominant loss mechanism. This prediction was borne out by measurements in which P_{Kr} was varied up to $\sim$50 Torr. These experiments substantiate the conclusion that the ionization rate dominates the quenching and spontaneous emission rates for most of the data in Fig. 5.

The clear quadratic variation of the photoelectron density for pressures as high as 50 Torr and I_{ArF} as low as $\sim$100 MW cm^{-2} allows one to examine condition (21) more closely. If $\tau_{sp}^{-1}=8.7\times10^6$ s^{-1} and $k_Q(6p[\frac{3}{2}]_2)=6.7\times10^{-10}$ cm^2 s^{-1} (Ref. 6) and assuming a reasonable value for σ_{PI} ($\leq10^{-18}$ cm^2), then (21) *will not be satisfied* for pressures as high and intensities as low as those observed experimentally. That is, if we consider the 50-Torr data, $\sigma_{\mathrm{PI}}I(\hbar\omega)^{-1}$ is apparently much greater than $\tau_{sp}^{-1}+k[\mathrm{Kr}]$ for $I_{\mathrm{ArF}}\gtrsim100$ MW cm^{-2}. For this value of intensity, $\sigma_{\mathrm{PI}}I(\hbar\omega)^{-1}\approx10^8$ s^{-1}, while the sum of the collisional and radiative rates is greater than 10^9 s^{-1}. Therefore, it appears that the rate constant for quenching of the $6p[\frac{3}{2}]_2$ state by Kr reported in Ref. 6 is too large by at least an order of magnitude. This conclusion is plausible for two additional reasons. Setser and co-workers[13,14] have measured the rate constants for quenching of the $Kr(5p)$ and $Xe(6p[\frac{1}{2}]_0,\ 6p[\frac{3}{2}]_2)$ states by the ground-state species. In the former case, the average value of k_Q for the five states studied is 1.2×10^{-10} cm^3 s^{-1} and none is larger than 2.7×10^{-10} cm^3 s^{-1}. For the latter, the rate constants were determined to be 5.8×10^{-12} and 8.2×10^{-11} cm^3 s^{-1}, respectively. Thus $k_Q(6p[\frac{3}{2}]_2)$ seems large in comparison with the measured constants for analogous rare-gas p states.

Second, the ArF laser in Ref. 6 was tuned to the two-photon $4p^6\,{}^1S_0\rightarrow6p[\frac{3}{2}]_2$ transition and line narrowed ($\Delta\tilde{\nu}\sim25$ cm^{-1}) by means of two prisms. With a source of such high spectral brightness, stimulated emission on a Kr $6p\rightarrow5s$ transition[15,16] makes it difficult to extract quenching rate constants even at low Kr pressures (<5 Torr). For the same reason, the Xe $6p[\frac{1}{2}]_0$ quenching rate constant reported in Ref. 15 is an upper limit.

The dashed line in Fig. 5 illustrates the cubic dependence of n_e on I_{ArF} for $p_{\mathrm{Kr}}=50$ Torr and ArF laser intensities below $\sim$100 MW cm^{-2}. If one assumes that k_Q is indeed on the order of 2×10^{-11} cm^3 s^{-1}, then the transition of n_e from a cubic to quadratic dependence on I_{ArF} would be expected to occur at $\sim$60 MW cm^{-2} for $p_{\mathrm{Kr}}=20$ Torr and at $\sim$47 MW cm^{-2} for the 10-Torr data.

B. Two-photon cross section

Assuming that photoionization is the dominant loss process for the $6p[\frac{3}{2}]_2$ state, Eq. (20) simplifies to

$$\frac{dn_e}{dt}\approx\frac{\sigma I^2}{\hbar\omega}[\mathrm{Kr}]\,. \tag{22}$$

The two-photon cross section σ that was presented in Sec. IV D was an *effective* value since it was measured with a broadband laser. In reality, of course, σ can be written

$$\sigma=\sigma_0 g(\omega)\,, \tag{23}$$

where σ_0 is the absorption cross section at line center and $g(\omega)$ is the two-photon line shape. Since both I and σ are functions of the frequency ω, Eq. (22) becomes[4]

$$\frac{dn_e}{dt}\simeq\frac{\sigma_0}{\hbar\omega_L}[\mathrm{Kr}]\int_0^\infty g(\omega)d\omega\int_0^\infty\gamma(\omega')\gamma(\omega-\omega')d\omega'\,, \tag{24}$$

where ω_L is the center frequency of the ArF laser, $\gamma(\omega')$ describes the spectral variation of the laser intensity [intensity expressed in (Hz)$^{-1}$ at ω'; $\int_0^\infty\gamma(\omega')d\omega'=I$, the total intensity], and the second integral [$\equiv I^{(2)}(\omega)$] is a measure of the number of two-photon pairs whose total energy is $\hbar\omega$, where $\int_0^\infty I^{(2)}(\omega)d\omega=I^2$. For the case of a Gaussian intensity distribution,

$$\gamma(\omega)=\left[\frac{2}{\pi}\right]^{1/2}\frac{I}{\Delta}\exp\left[-2\left[\frac{\omega-\omega_L}{\Delta}\right]^2\right] \tag{25}$$

and

$$I^{(2)}\omega=\frac{I^2}{\sqrt{\pi}\Delta}\exp\left[-2\left[\frac{\omega-2\omega_L}{\sqrt{2}\Delta}\right]^2\right]\,, \tag{26}$$

where Δ is the spectral *full width* at half maximum (FWHM) of the laser pulse divided by $\sqrt{2\ln2}$.

If the atomic line shape is also Gaussian ($g(\omega)=\exp\{-2[(\omega-\omega_0)/\delta]^2\}$), where δ is the FWHM of the atomic absorption line divided by $\sqrt{2\ln2}$, then Eq. (24) can be rewritten

$$\frac{dn_e}{dt}\simeq\frac{\sigma_0[\mathrm{Kr}]I^2}{\hbar\omega_L}\frac{\delta}{\sqrt{2\Delta^2+\delta^2}}\exp\left[-2\frac{(2\omega_L-\omega_0)^2}{2\Delta^2+\delta^2}\right]\,. \tag{27}$$

Since the laser bandwidth is much larger than the atomic linewidth, Eq. (27) can be simplified to

$$\frac{dn_e}{dt} \simeq \frac{\sigma_0[\mathrm{Kr}]I^2}{\hbar\omega_L} \frac{\delta}{\sqrt{2}\Delta} \exp\left[-\left[\frac{2\omega_L - \omega_0}{\Delta} \right]^2 \right] . \quad (28)$$

Although this analysis has not considered the effect of Doppler or pressure broadening, its inclusion would only result in the addition of other linewidth terms to the denominator of the exponent in (27) and the laser bandwidth Δ still dominates. By comparing Eq. (28) with Eq. (3), it is seen that neglecting the frequency dependence of two-photon absorption results in a cross section which is a factor of $(\sqrt{2}\Delta/\delta)\exp\{[(2\omega_L - \omega_0)/\Delta]^2\}$ too small.[4] For $\delta \simeq 300$ MHz (Ref. 17), $\Delta = 4$ THz, and $2\omega_L - \omega_0 = 2.1$ THz as in these experiments, the absorption cross section given in Sec. IV becomes 5×10^{-28} cm^4 W^{-1}. This value is similar in magnitude to that measured by Gornik *et al.*[18] for the two-photon excitation of the Xe $6p[\frac{3}{2}]_2$ state with a frequency-doubled dye laser ($\alpha \simeq 1.2 \times 10^{-27}$ cm^4 W^{-1}).

VI. CONCLUSIONS

The effective two-photon ionization cross section describing the resonantly enhanced three-photon ionization of krypton at 193 nm has been measured to be 2×10^{-32} cm^4 W^{-1} for an ArF laser with a bandwidth (FWHM) of 140 cm^{-1}. This corresponds to an absorption cross section of 5×20^{-28} cm^4 W^{-1} for an atomic linewidth (FWHM) of 300 MHz. Both values are in agreement with experimentally measured and calculated cross sections in the literature. Unlike previous experimental determinations of cross sections, the approach pursued here exploits inverse bremsstrahlung to observe (in real time) the absolute electron number density produced during the photoionization process.

ACKNOWLEDGMENTS

The authors are grateful for the technical assistance of K. Kuehl, Y. Moroz, C. Zeitkiewicz, P. Hayes, and D. Watterson. This work was supported by the National Science Foundation (R. E. Rostenbach) under Grants No. CPE 82-07868 and No. CPE 82-19295.

*Present address: Laser Physics and Applications Group, MS E543, Los Alamos National Laboratory, Los Alamos, NM 87545.

[1]A. W. McCown, M. N. Ediger, and J. G. Eden, Phys. Rev. A **26**, 3318 (1982), and Refs. 11 and 23 cited therein.

[2]Measurements in this laboratory in which 300 Torr of Kr was irradiated by 800-mJ, 15-ns FWHM pulses of 248-nm (KrF) radiation produced no detectable electrons by microwave absorption. Therefore, $n_e \lesssim 10^9$ cm^{-3} and the *upper limit* for the nonresonant three-photon ionization cross section for Kr at 248 nm is estimated to be 3×10^{-45} cm^6 W^{-2}.

[3]E. J. McGuire, Phys. Rev. A **24**, 835 (1981).

[4]See, for example, B. R. Marx, J. Simons, and L. Allen, J. Phys. B **11**, L273 (1978), and references cited therein.

[5]W. K. Bischel, J. Bokor, D. J. Kligler, and C. K. Rhodes, IEEE J. Quantum Electron. **QE-15**, 380 (1979); D. Kligler, D. Pritchard, W. K. Bischel, and C. K. Rhodes, J. Appl. Phys. **49**, 2219 (1978).

[6]J. Bokor, J. Zavelovich, and C. K. Rhodes, Phys. Rev. A **21**, 1453 (1980).

[7]M. S. Pindzola, M. G. Payne, and W. R. Garrett, Phys. Rev. A **24**, 3115 (1981).

[8]A. W. McCown, M. N. Ediger, and J. G. Eden, Phys. Rev. A **29**, 2611 (1984).

[9]D. B. Geohegan, A. W. McCown, and J. G. Eden, J. Chem. Phys. **81**, 5336 (1984).

[10]J. C. Miller, A. E. Carter, and P. Kruit, Chem. Phys. Lett. **71**, 87 (1980).

[11]L. S. Frost and A. V. Phelps, Phys. Rev. **136**, A1538 (1964).

[12]T. N. Chang and Y. S. Kim, Phys. Rev. A **26**, 2278 (1982).

[13]R. S. F. Chang, H. Horiguchi, and D. W. Setser, J. Chem. Phys. **73**, 778 (1980).

[14]D. W. Setser and J. Ku, in *Proceedings of the Conference on Photochemistry and Photophysics above 6 eV,* Societe Francaise de Chimie, France, 1984 (unpublished).

[15]A. W. McCown, M. N. Ediger, and J. G. Eden, Phys. Rev. A **26**, 2281 (1982).

[16]T. D. Raymond, N. Bowering, C.-Y. Kuo, and J. W. Keto, Phys. Rev. A **29**, 721 (1984).

[17]Estimated for a Kr pressure of 20 Torr from Ref. 18 and O. Vallée, E. Marié, N. Tran Minh, and R. Vetter, Phys. Rev. A **24**, 1391 (1981).

[18]W. Gornik, S. Kindt, E. Matthias, and D. Schmidt, J. Chem. Phys. **75**, 68 (1981).

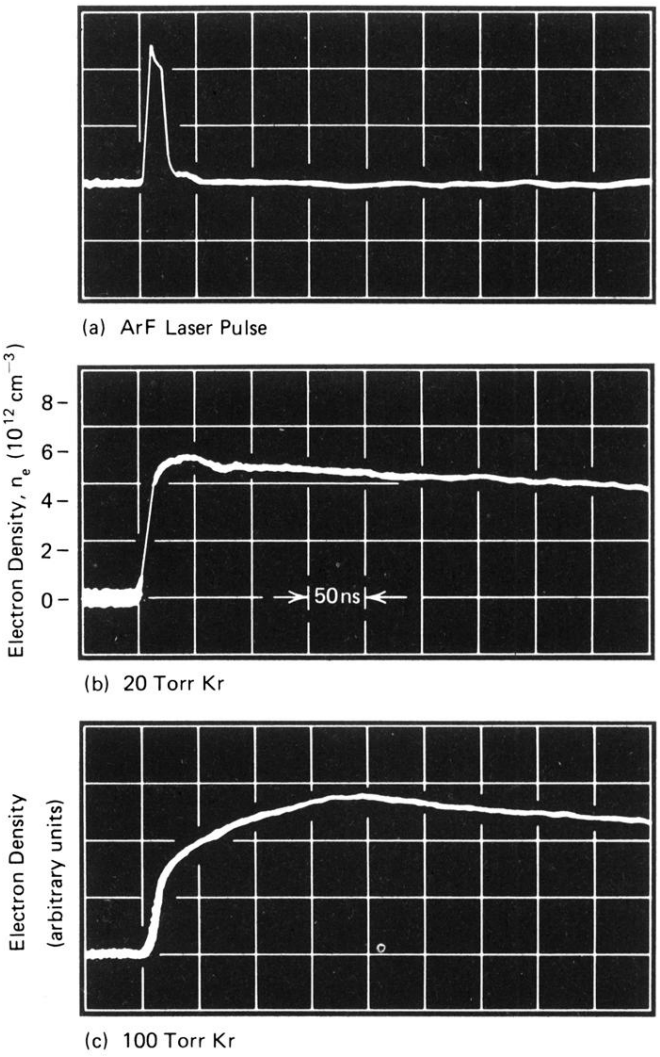

FIG. 3. Laser (a) and microwave-attenuation (b), (c) waveforms observed in these experiments. In (b) and (c) electron density increases vertically, and for Kr pressures beyond ~ 50 Torr, the influence of metastable-metastable collisions on electron production is clearly evident.